AIP | Biomicrofluidics
Fundamentals, Perspectives & Applications

On-chip microfluidic biosensor using superparamagnetic microparticles

G. Kokkinis, F. Keplinger, and I. Giouroudi

Citation: Biomicrofluidics **7**, 054117 (2013); doi: 10.1063/1.4826546
View online: http://dx.doi.org/10.1063/1.4826546
View Table of Contents: http://scitation.aip.org/content/aip/journal/bmf/7/5?ver=pdfcov
Published by the AIP Publishing

On-chip microfluidic biosensor using superparamagnetic microparticles

G. Kokkinis, F. Keplinger, and I. Giouroudi[a)]
Institute of Sensor and Actuator Systems, Vienna University of Technology, Gusshausstrasse 27-29/366-ISS, Vienna 1040, Austria

(Received 1 August 2013; accepted 10 October 2013; published online 21 October 2013)

In this paper, an integrated solution towards an on-chip microfluidic biosensor using the magnetically induced motion of functionalized superparamagnetic microparticles (SMPs) is presented. The concept of the proposed method is that the induced velocity on SMPs in suspension, while imposed to a magnetic field gradient, is inversely proportional to their volume. Specifically, a velocity variation of suspended functionalized SMPs inside a detection microchannel with respect to a reference velocity, specified in a parallel reference microchannel, indicates an increase in their non-magnetic volume. This volumetric increase of the SMPs is caused by the binding of organic compounds (e.g., biomolecules) to their functionalized surface. The new compounds with the increased non-magnetic volume are called loaded SMPs (LSMPs). The magnetic force required for the manipulation of the SMPs and LSMPs is produced by current currying conducting microstructures, driven by a programmable microcontroller. Experiments were carried out as a proof of concept. A promising decrease in the velocity of the LSMPs in comparison to that of the SMPs was measured. Thus, it is the velocity variation which determines the presence of the organic compounds in the sample fluid. © *2013 AIP Publishing LLC*. [http://dx.doi.org/10.1063/1.4826546]

I. INTRODUCTION

Integrated microfluidic platforms used in micro-total analysis systems (μTAS) have remarkable advantages over laboratory operated devices in terms of sample and reagent volume decrease, minimization of human intervention, and cost reduction.[1,2] Labeling of biological entities or organic compounds with superparamagnetic microparticles[3] (SMPs) for biomolecular recognition is successfully implemented in bioanalytical investigations.[4,5] Suspensions of SMPs can be magnetized by external magnetic fields enabling the controlled manipulation or related properties of SMPs like concentration, separation, trapping, and transportation as well as their detection by means of magnetic sensors.[5–8] Using magnetic methods for the aforementioned tasks has several advantages; magnetic fields can be well tuned and applied either externally or by a directly integrated solution in the microfluidic system, and SMPs are ideal candidates as the active component in miniaturized on-chip diagnostic systems due to their multifunctionality.[9–15]

Methods for magnetic manipulation of SMPs have been demonstrated in several previous studies striving towards the production of magnetic field gradients, steep enough, to move SMPs towards a desired direction or sensing area.[16–18] Conventional methods use permanent magnets to generate the magnetic force. The main drawback of this approach is the difficulty to obtain a well-defined force. In this research work we developed an integrated solution for the application of the magnetic field gradient; parallel conducting microstructures were designed, fabricated and current was sequentially applied to them by a programmable microcontroller. This method provided adequate magnetic field gradients ensuring a better control over the

[a)]Author to whom correspondence should be addressed. Electronic mail: ioanna.giouroudi@tuwien.ac.at

SMPs' motion. A novel concept is presented, which exploits the advantages of SMPs for the qualitative detection of organic compounds, e.g., biomolecules. Experiments for the proof of concept are reported and discussed.

II. WORKING PRINCIPLE AND CALCULATIONS

The proposed microfluidic biosensing method is based on the volumetric increase of functionalized SMPs due to the binding of non-magnetic compounds onto their surface (LSMPs). This leads to a consequent decrease in the velocity of the LSMPs with respect to SMPs provided that both LSMPs and SMPs are subjected to identical magnetic forces.[14,19] Specifically, the chip consists of a reference microchannel and a detection microchannel. In the reference microchannel plain SMPs are injected having a certain volume V and a diameter D. The fluid which contains the plain SMPs has the same viscosity as the fluid under investigation (sample fluid). In a second step the sample fluid containing the organic compounds (e.g., biomolecules) is mixed with functionalized SMPs. The resulting sample fluid contains the LSMPs which have an increased volume V' and diameter D' in comparison to the SMPs in the reference microchannel. Afterwards, the resulting sample fluid is inserted in the detection microchannel. Then, current is applied sequentially at the microstructures. This causes a magnetic force to act on the SMPs and the LSMPs, and therefore the SMPs and LSMPs move through the reference and detection microchannel along the x-axis, respectively. Fig. 1(a) shows the fabricated microfluidic chip.

In general, in order to use a magnetic field to move SMPs, a magnetic field gradient is required to exert a translational force. This dominant magnetic force exerted on an SMP (F_m) is expressed as[20]

$$\vec{F}_m = \frac{V_b \Delta\chi}{\mu_0} \vec{B}(\vec{\nabla} \cdot \vec{B}), \tag{1}$$

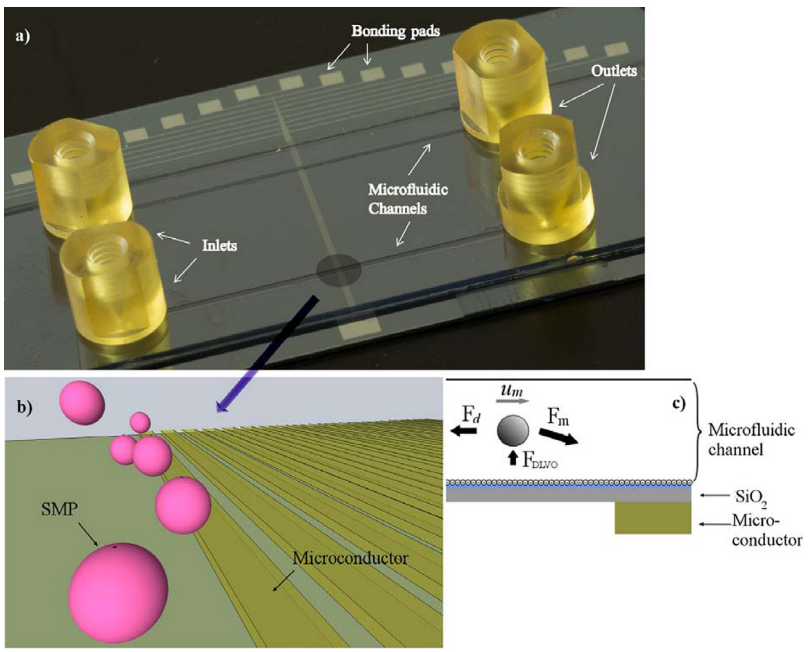

FIG. 1. (a) Photograph of the proposed microsystem consisting of two microfluidic channels: the detection and the reference microchannels, inlet and outlet connectors and bonding pads for wire bonding. (b) Schematic illustration of the microchannel at the intersection with the parallel conducting microstructures and the SMPs. (c) Forces exerted on a single SMP: the magnetic force F_m, the hydrodynamic drag force F_d, and the repulsive DLVO forces (consisting mainly of the van der Waals and the electrostatic interaction forces) F_{DLVO}. The net force defines the translational movement of the particles at the direction of the particles velocity, u_m.

where V_b is the volume of the SMP, μ_0 is the permeability of the vacuum ($4\pi \times 10^{-7}$Vs/Am), $\Delta\chi$ is the difference of magnetic susceptibilities between the SMP and the surrounding medium (in our case water or buffer solutions), and B is the magnetic flux density.

It can be seen from Eq. (1) that the force on an SMP is directly proportional to both the magnitude of the magnetic field and its gradient. Hence, in order to effectively manipulate the SMPs, the magnetic field can be increased given that the SMPs' magnetization is not saturated and/or the magnetic gradient can be enhanced. This makes it obvious that the only realistic way of maximizing the magnetic force is by miniaturizing the magnetic field source. The small size of the conducting microstructures strongly enhances the magnetic field gradient and therefore produces large and tunable magnetic forces that can be applied on the SMPs.

There are several other forces acting on suspended particles such as colloidal, electrostatic, and hydrodynamic forces.[21,22] Double-layer electrostatic and van der Waals forces are commonly referred to as DLVO forces,[21] named after the scientists that first described them in detail (Derjaguin, Landav, Verwey, Overbeek). According to Ref. 23 a layer of SiO_2 produces a negatively charged surface in aqueous buffer, thus producing a repulsive force between negatively charged particles and the solid surface (see Fig. 1(c)). In consequence, by enhancing the electrostatic repulsive component and maintaining the van der Waals attractive force constant, the net DLVO force is a counterforce to the y-component of the magnetic force F_m and can be used to avoid particle-solid surface adhesion.

The hydrodynamic force is the strongest competing to the magnetic force and is, for the presented application, the one responsible for the velocity change in respect to volumetric increase. This frictional force, known as Stokes' drag, acting on the interface between the fluid and the SMP, for small Reynolds numbers and for spherical SMPs, is given by the equation[24]

$$\vec{F}_d = 3\pi D\eta\upsilon, \tag{2}$$

where D is the diameter of the SMP, η is the viscosity of the medium, and υ is the relative velocity of the fluid with respect to the SMP. The Stokes drag is applicable to the creeping flow regime (Stokes regime) with small Reynolds numbers ($\mathrm{Re} < 0.5$).

As it will be shown below, the volumetric increase can be achieved by the conjugation of biomolecules or other non-magnetic particles on the surface of the functionalized SMPs. Equation (3) is often used to approximately calculate the drag force exerted on conjugated particles. The reason is that biomolecules rarely bind around the whole surface of an SMP so as to accurately apply Eq. (3). Instead, a cluster of two or more biomolecules on the SMP is formed (as shown in Fig. 2). Thus a more accurate form of Eq. (3) can be used[25]

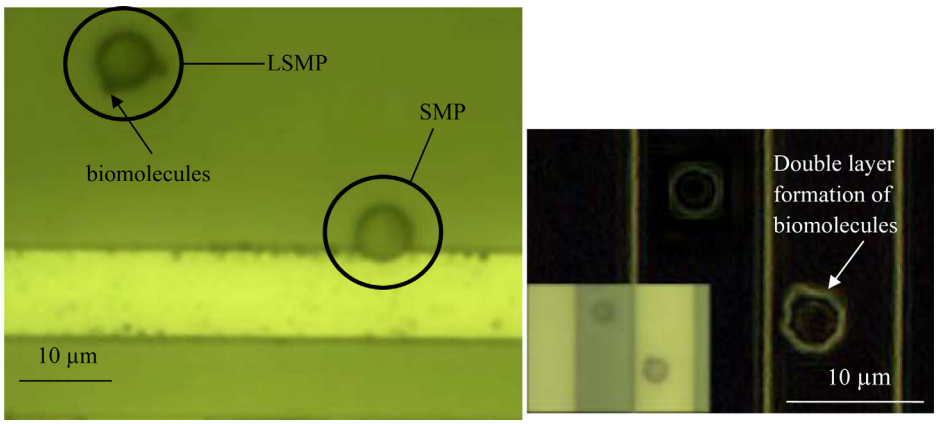

FIG. 2. (a) Microscope photo of a 6 μm magnetic particle SMP and a compound LSMP consisting of a 6 μm functionalized SMP and 1 μm biomolecules attached to its surface. (b) Detailed photo showing the formation of a double layer of conjugated biomolecules.

$$\vec{F}_d = 3\pi D_e \eta \upsilon K, \tag{3}$$

where D_e is the diameter of a sphere having the same volume as the cluster of particles. That is,

$$D_e = \left(\frac{6}{\pi} Volume\right)^{1/3}, \tag{4}$$

and K is the correction factor which for tightly packed clusters, like in our case,[26] is $K = 1.12$.

Based on Eqs. (2)–(4), we calculated the percent decrease of velocity for SMP of different diameters and attached biomolecules of different diameters, as shown in Fig. 3, in order to compare it afterwards to the experimental results (Sec. IV).

An additional parameter that considers the hydrodynamic size of an SMP, apart from its physical size, is the electrical double layer around it. The electrical double layer is formed due to the surface charge acquired by an SMP through the adsorption of ions present in the solution and/or due to the presence of charged surface groups, as well as due to the oppositely charged mobile ions that neutralize this surface charge.[27] In this work, the double layer was insignificant compared to the physical size of the SMPs (>250 nm in diameter). For the SMPs used in the presented experiments the hydrodynamic size was assumed to be equal to the physical size.

III. METHODS AND FABRICATION

A. Simulations

The design and the materials used for the microfluidic biosensor as well as the SMPs used for the experiments were decided upon numerical simulations of the magnetic field generated by the microstructures, the medium creeping flow, the SMP trajectories, and the thermal analysis of the device. The simulations were carried out using the commercial software COMSOL®, solving the Maxwell's differential equations for the magnetic flux, the Navier-Stokes differential equations for the creeping flow—wherever applicable—and the Newton's second law of motion for acquiring the particle trajectories. All the studies were time dependent.

Two possible geometries of the conducting microstructures were first investigated: circular conductors and parallel conductors (see Fig. 4). A long-range displacement of magnetic particles can be assured by arranging adjacent ring type conductors in an array with spatial overlap.[28–31] A 3D model was necessary for simulating the magnetophoretic capability of this type of circular conductors. As illustrated in Fig. 4(a), the advantage of the arrangement lies on

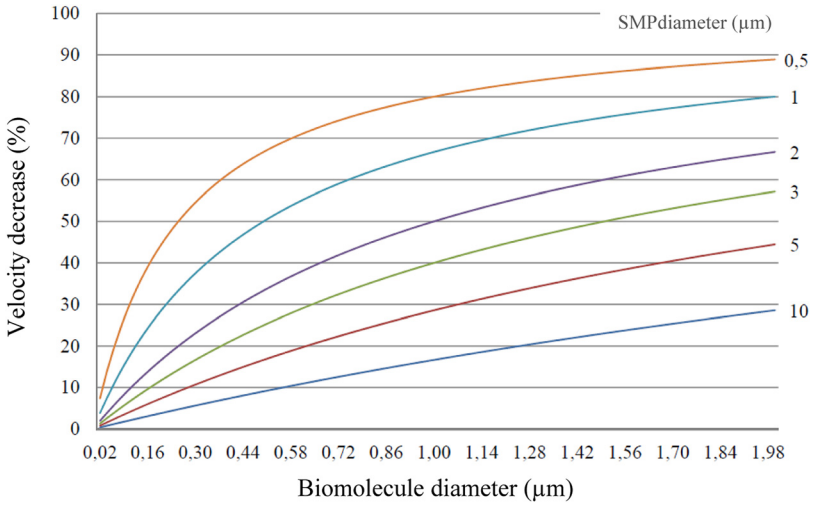

FIG. 3. Percent velocity decrease of an LSMP compared to the plain SMP with respect to the biomolecule diameter.

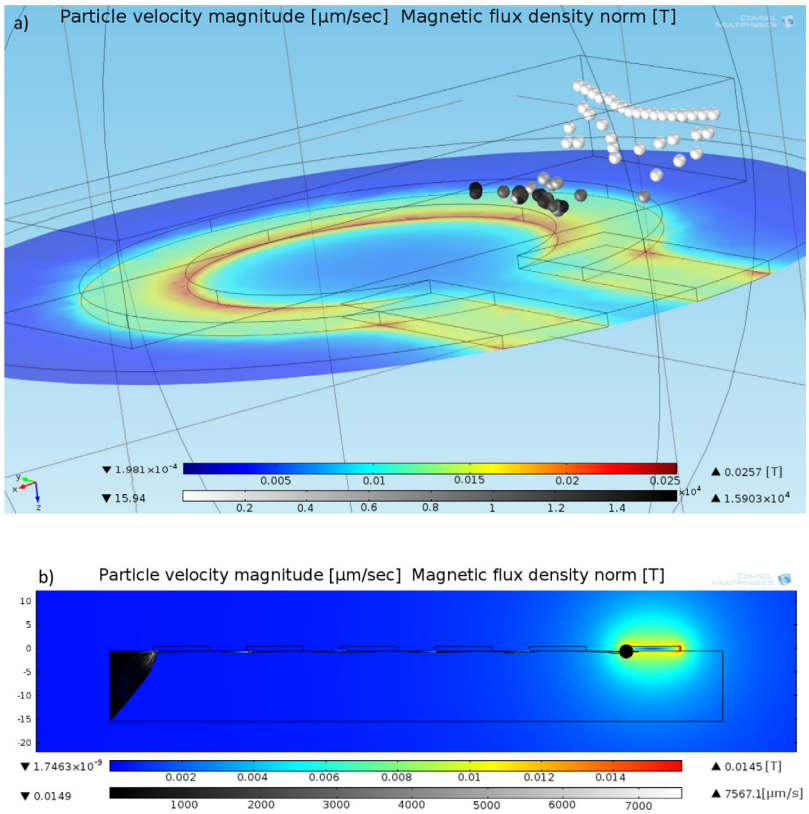

FIG. 4. The magnetic flux density generated by the conducting microstructures carrying a current of 100 mA and the SMPs' trajectories for two different designs. (a) 3D model of a single ring type conducting microstructure with magnetic particles suspended in a microfluidic channel with no flow. The image illustrates the non-uniform velocity profile of the particles as well as the concentration of the magnetic flux at the inner edge of the ring. (b) 2D model of six parallel microconductors with current sequentially applied to them, at the moment the sixth conductor is switched on. The trajectories are represented with a continuous line causing the black shape to appear at the beginning of the channel, as the particles are considered evenly distributed at the inlet.

concentrating the magnetic flux density at the inner side of the loop while for the parallel conductors the magnetic flux density picks at both edges (Figs. 4(b) and 5(a)). In favor of a more simplified design the parallel conducting microstructures were investigated using a 2D model, saving both time and computing power. This parallel arrangement guarantees identical magnetic field in both channels, as well as homogeneous velocity profiles for SMPs in the same channel. Conclusively, the parallel conductor design was adapted for fabrication.

In order to evaluate different conductors' width and spacing, a key parameter had to be kept constant. That was the current density. A silicon chip can tolerate current densities up to 10^{14} A/m^2; hence, the limiting factor in microdesign is no longer the melting point of the conducting microstructures' material but rather the occurrence of electromigration, a phenomenon that occurs in conducting microstructures stressed under high current densities. This might result in a steady change of conductor dimensions, thereby causing the creation of either voids or the creation of hillocks and whiskers in the affected regions. Both can eventually lead to the failure of the circuit. In our case, though, what is even more important is maintaining a low temperature on the chip, for protein and other biomolecules, denaturation prevention. For that purpose a 3D Joule heating model was designed, with a time dependent study. The time interval for which current was applied at the conducting microstructures depends on their width and spacing (see Fig. 1(b)). Setting an upper temperature limit at 323 K, the numerical simulation indicated a maximum current density of 9 A/m^2.

Taking all the above into consideration as well as limitations during fabrication, the optimum dimensions for the parallel conducting microstructures made of silver (Ag) were defined

as 10 μm in width, 500 nm thickness, and 8 μm spacing. For the simulations, a current of 100 mA was applied in a sequential pattern and a time dependent solution was calculated. Fig. 5(a) shows the distribution of the magnetic field on a cut edge of the 2D model and Fig. 5(b) the magnetic force acting on a Micromod Sicastar® magnetic particle of 1.5 μm radius, susceptibility of $\chi_m = 0.189$ and magnetic volume of 1.77×10^{-18} m^3. The magnetic field, which is highest at the edges, is strongly localized and drops about 83% at a distance of 10 μm from the edges. The peak force exerted on a particle is approximately 2 pN.

B. Microfluidic device fabrication

The system consisted of the Ag conducting microstructures, the microfluidic channels, the SMPs, and the LSMPs. The conducting microstructures were fabricated with standard photolithography techniques. The substrate of the device was a commercial silicon 100 mm wafer, 500 μm thick with a 1.6 μm thick layer of thermally grown oxide.

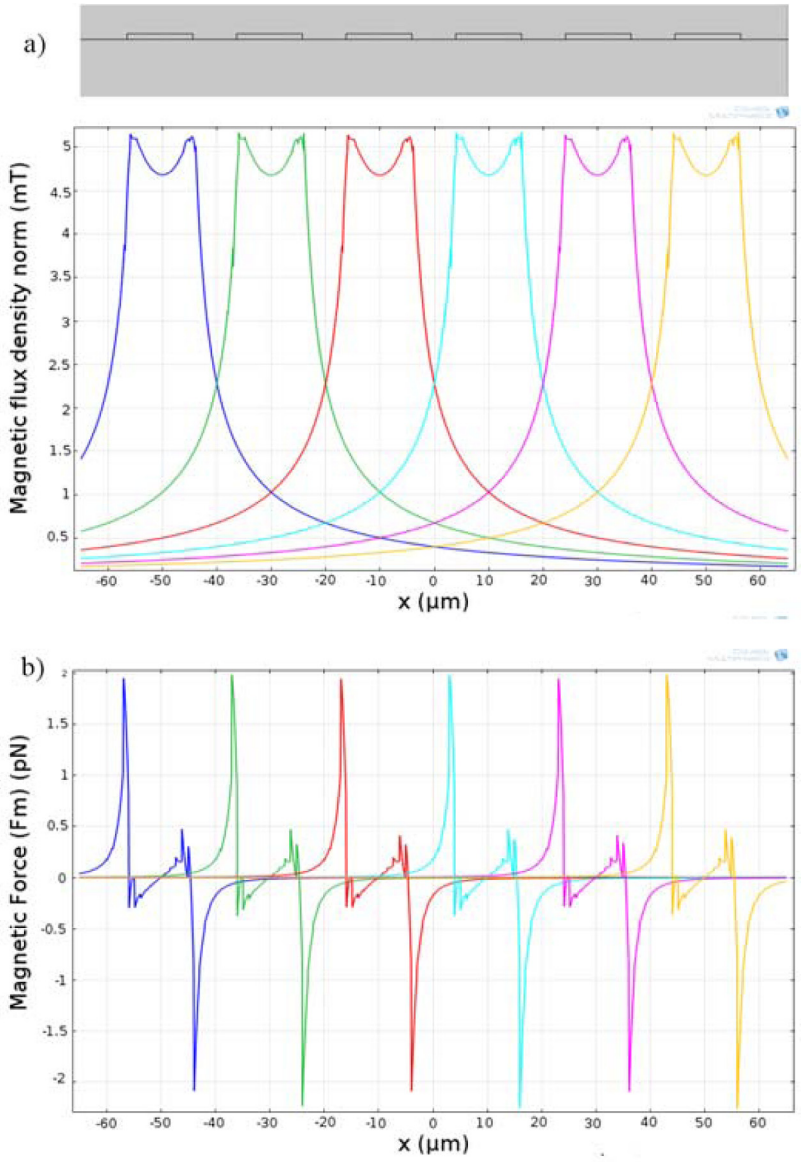

FIG. 5. (a) Numerical results for the magnetic flux density of 6 parallel conducting microstructures (width $w = 10$ μm and spacing $s = 8$ μm) along a cut line 1 μm away from the conducting microstructures. (b) The magnetic force exerted on an SMP of 1.5 μm radius and susceptibility of $\chi_m = 0.19$ along the same cut line.

First, both the wafer and the chromium pattern mask were cleaned with deionized (DI) water rinse and megasonic actuation. Then the wafer was prebaked at 120 °C for 2 min to remove water and to improve adhesion of the photoresist. Spin coating of a 1.62 μm thick layer of the AZ 5214® image reversal photoresist was achieved at 3000 rpm. A prebake at 107 °C for 2 min was necessary for evaporating the solvent, and a thin layer of AZ Aquatar® was spinned on to prevent reflections and stiction of the chromium mask on the wafer. An additional prebake step at 107 °C for 2 min was carried out. Then the wafer was exposed in a Karl Suss MA-150 Mask Aligner for 2 s followed by an image reversal bake at 120 °C for 2 min, 20 s of flood exposure and development of the photoresist using the AZ 351B® developer by spraying it on the wafer for 60 s while spinning at 3000 rpm. The developer was then removed by rinsing the wafer with DI water. The structured substrate was then placed into the vacuum chamber for the thermal evaporation of 50 nm titanium, 400 nm of silver, and 50 nm of chromium. Titanium was necessary for the adhesion of silver. Chromium was used for protection of the silver against corrosion caused by the following step of the lift-off process and the silicon dioxide deposition. The lift-off process took place in three successive acetone baths. A passivation layer was essential for electrical insulation, electrostatic interaction with SMPs, and future surface modifications. Silicon dioxide meets all these demands; thus, a 300 nm layer was formed on top of the structures, by employing Plasma Enhanced Chemical Vapor Deposition (PECVD). Utilizing the Oxford Plasma Lab 100 system at a low temperature (120 °C) and pressure of 6 mTorr, with a forward power of 1500 W and a gas flow rate of 40 sccm for N_2O and 5 sccm SiH_4, we obtained a SiO_2 layer with a refractive index $n = 1.426$. On the following step, the pads for wire bonding were released; a layer of positive photoresist was used as protective mask, and the whole wafer was plasma etched for 10 min, at 50 mTorr pressure and 180 V forward voltage in STS 320PC plasma etcher. The flow rates were set at 6 sccm for O_2 and at 85 sccm for CHF_3.

After the conducting microstructures were fabricated, the microfluidic channels were structured. For this purpose a 55 μm thick, negative type, dry-film, photoresist (Ordyl®) was used. First, the wafer was cleaned, to remove any contamination from the previous treatments, by immersing it in a 10% RBS 50 basic solution in DI water at 50 °C and under ultrasonic actuation. Before lamination it was dried for 30 min at 120 °C. For the next step a standard office laminator was used, with hot rolls being set at 70 °C. A 25 s exposure was performed using a Karl Suss MA-150 Mask Aligner followed by a 60 s post exposure bake at 80 °C on a hot plate. The exposed photoresist was developed for 1.5 min in 3 successive baths of increasing cleanness and rinsed with isopropanol and DI water.

The final step was the sealing of the channels and the drilling of the inlet and outlet holes. For that purpose a standard 100 mm glass wafer was drilled using a Computer Numerical Control (CNC) diamond drilling system. After cleaning it, in the aforementioned solution, it was thermally bonded on the Ordyl® structures, in an EVG 501 wafer bonder, by applying a force of 60 N/cm^2 of photoresist. The temperature was increased to 100 °C with a 5 °C/min ramp and maintained for 30 min. Afterwards, the temperature was reduced to room temperature at 1 °C/min. To cut the bonded wafers into single chips a DAD 3220 dicing saw with a 200 μm thick diamond blade was used. The inlet and outlet holes in the glass-wafer were sealed with adhesive tape before dicing to prevent cooling water and debris from entering the chips. To free the contact pads, the glass wafer was partially removed in the areas above the pads. This was performed by dicing the chip half through; dicing only through the glass-wafer and using the Ordyl® layer as a spacer that prevented the conducting microstructures and contact pads from getting damaged.

IV. EXPERIMENTS

In order to prove the concept of velocity decrease due to volumetric increase of functionalized SMPs we used Micromer®-M-PEG-COOH (3 μm and 6 μm diameter, respectively) magnetic microparticles with carboxyl groups (-COOH) protruding from the surface and Micromer®-NH_2 (500 nm and 1 μm diameter, respectively) non-magnetic polymer particles with

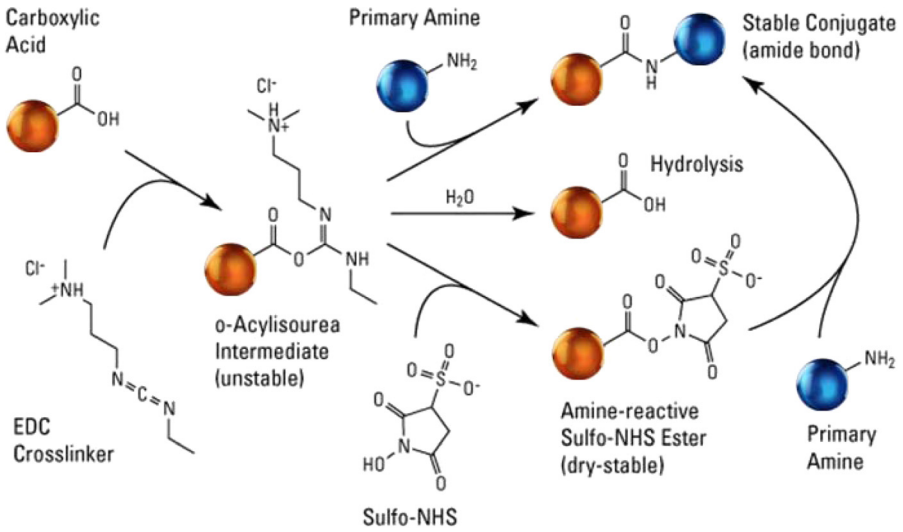

FIG. 6. Carboxyl-to-amine crosslinking reaction scheme using the carbodiimide EDC and sulfo-NHS. Addition of NHS or Sulfo-NHS to EDC reactions (bottom-most pathway) increases efficiency and enables the SMP with the carboxylic acid group to be activated for storage and later use.

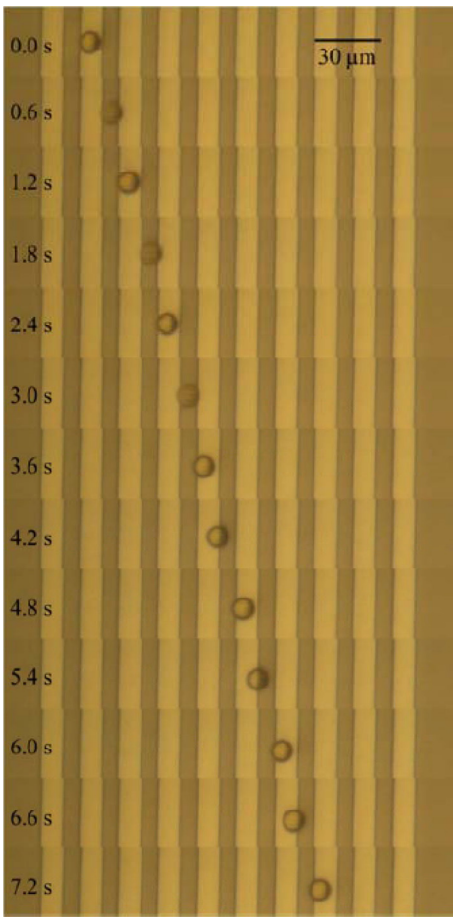

FIG. 7. Movement of a micromer® 10 μm SMP along the microfluidic channel with an actuation time of 1.2 s per conducting microstructure (geometry: width = 10 μm, spacing = 8 μm). The current was I = 50 mA. The SMP covered a distance of 108 μm with a mean velocity of 15μm/s.

amino groups (-NH_2) protruding from the surface. The particles were mixed following the protocol given by the provider, and a bond was achieved between magnetic, carboxyl group coated SMPs and non-magnetic, amino group coated polymer particles (as shown in Fig. 6). This way, LSMPs were formed leading to an increased volume of the carboxyl group coated SMPs. It was found that the particle-particle bonding worked quite well.

The movement of the LSMPs in comparison to the movement of the SMPs caused by the applied magnetic field from the conducting microstructures was demonstrated optically by means of a microscope with a mounted CCD camera.[21] Several images and movies of the experiments were obtained. 50 mA current was applied sequentially to the conducting microstructures, employing a programmable microcontroller utilized to drive power MOSFETs; the actuation time depends on the size of the SMP.

Three sets of experiments were carried out; during the first set we confirmed the motion of SMPs without flow and only by application of a magnetic field generated from the Ag conducting microstructures. Specifically, Fig. 7 shows the movement of a 10 μm SMP from micromer® along the x-axis of the detection microchannel with a determined actuation time of 1.2 s. The position of the SMP is pictured every 0.6 s travelling a distance of 108 μm with a mean velocity of 15 μm/s.

During the second set, we proved the velocity change due to volumetric change. Specifically, 3 μm in diameter carboxyl group coated SMPs were injected in the reference microchannel and were moved towards the outlet with an actuation time of 3.8 s resulting to a mean velocity of 5.3 μm/s. Then the LSMPs (micromer®-M-PEG-COOH conjugated with 500 nm non-magnetic particles) were inserted in the detection microchannel. The predetermined actuation time was not adequate to transport the LSMPs; thus, it had to be increased to 6.8 s leading to a mean velocity of 2.94 μm/s. The optical realization of the experiment is seen in Fig. 8.

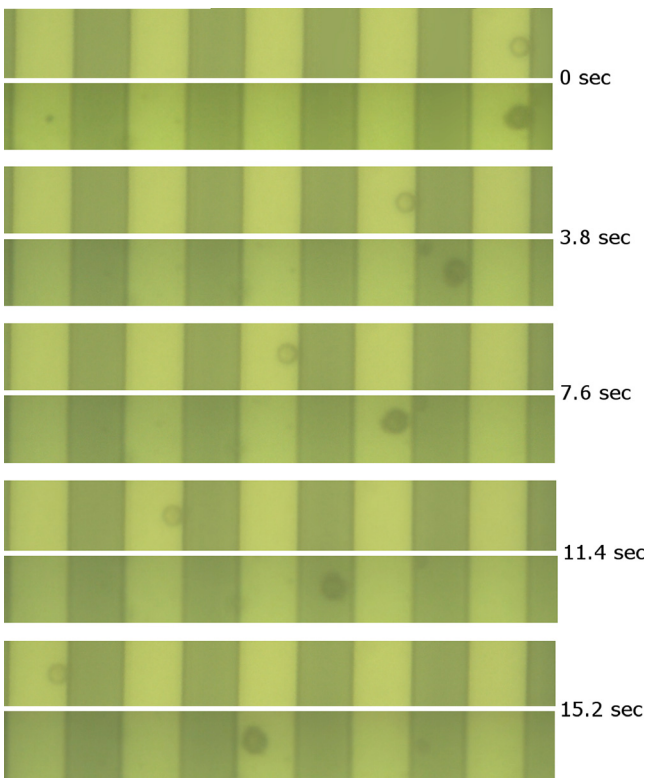

FIG. 8. Comparison of the plain micromer®-M-PEG-COOH 3 μm SMP in the reference channel and the LSMP consisting of 3 μm SMP conjugated with 500 nm non-magnetic particles travelling in the detection channel, actuated by a current of I = 50 mA. Actuation times are 2.3 s for the SMP and 3 s for the Loaded SMP.

The experiment showed a velocity reduction of about 44% for the LMNP against the plain MNP, while the theoretical velocity reduction was calculated to be 25% for an LMNP consisting of a 3 μm MNP plus attached 500 nm analyte compared to a plain 3 μm MNP. This relatively great deviation from the theoretical value can be attributed to the large number of non-magnetic particles conjugated to the magnetic one. As Figs. 2(b) and 8 demonstrate there are double layers of conjugated non-magnetic particles increasing even more the volume as well as several points of contact between the particles and the conductor's surface aggravating friction and possibly colloidal forces.

During the third set of experiments we proved that, regardless the size of the SMPs, if non-magnetic biomolecules are attached to their surface causing a volumetric increase a velocity decrease will always occur, if accelerated by a magnetic field without flow. Specifically, we used plain micromer®-M-PEG-COOH 6 μm SMPs and injected them in the reference microchannel. Afterwards, by sequentially applying current to the conducting microstructures we moved them towards the outlet with an actuation time of 3.2 s resulting to a mean velocity of 6.25 μm/s (similarly to the second set of experiments). Then LSMPs (consisting of 6 μm micromer®-M-PEG-COOH conjugated with 1 μm non-magnetic particles) were inserted in the detection microchannel. The predetermined actuation time was not adequate to transport the LSMPs; thus, it had to be increased to 5 s leading to a mean velocity of 4 μm/s. The optical realization of the experiment is seen in Fig. 9.

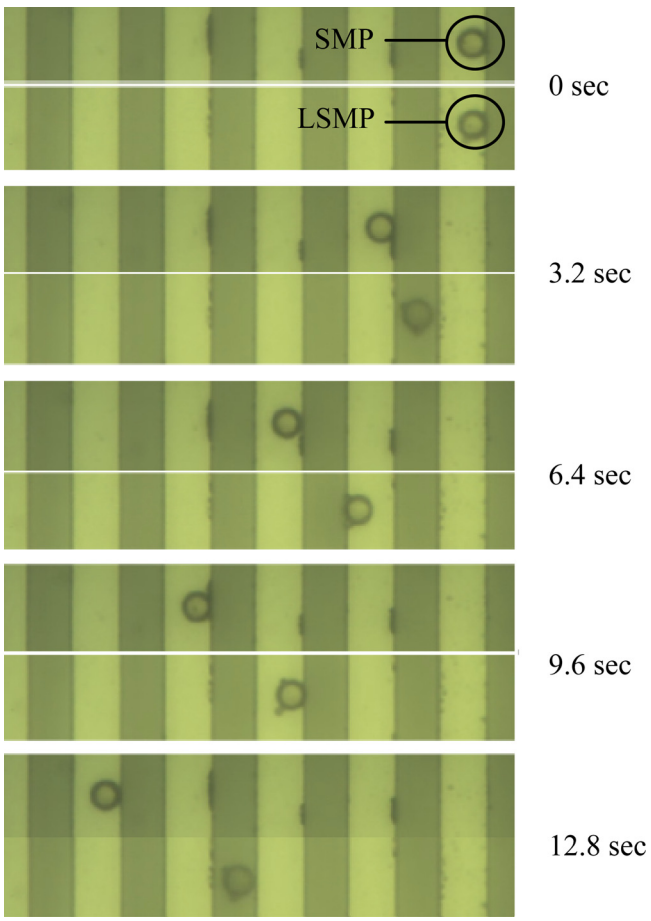

FIG. 9. Comparison of the plain micromer®-M-PEG-COOH 6 μm SMP in the reference channel and the LSMP consisting of 6 μm SMP conjugated with 1 μm non-magnetic particles travelling in the detection channel, actuated by a current of I = 50 mA. Actuation times are 3.3 s for the SMP and 5 s for the LSMP.

The experiment showed a velocity reduction of about 36% for the LSMP against the reference SMP. The theoretically calculated velocity reduction was 28% for an LSMP consisting of a 6 μm SMP plus 1 μm attached biomolecule compared to a plain 6μm SMP. In that case, as Figs. 2(a) and 9 demonstrate, the deviation from the theoretical value is not that great since a lesser percentage of the outer surface is covered by non-magnetic particles.

In order to ensure that regardless the number of repetitions, the velocity of the SMPs always decreases when biomolecules are attached to their surface, thus increasing their non-magnetic volume, we repeated the measurements for several counts and calculated the mean velocity of the SMPs without and with increased volume (as shown in Figs. 10–13). Specifically, Fig. 10 shows that for 6 μm SMPs, after 17 repetitions of the experiment, the statistical mean of the mean velocity was approximately 6.43 μm/s with a standard deviation of ~0.67 and the median value equal to 6.25 μm/s. Fig. 11 shows that for LSMPs consisting of 6 μm SMPs and 1 μm non-magnetic attached particles, after 50 repetitions the statistical mean of the mean velocity was approximately 3.83 μm/s with a standard deviation of ~0.83 and the median value equal to 4 μm/s. The same set of repetitive experiments was carried out for 3 μm SMPs (after 23 repetitions), as shown in Fig. 12, and for LSMPs consisting of 3 μm SMPs and 0.5 μm non-magnetic attached particles (after 40 repetitions), as shown in Fig. 13. Taking these results into consideration we can safely state that a non-magnetic volumetric increase of SMPs always leads to a velocity decrease. Therefore, by using our biosensing method, once a velocity decrease of the functionalized SMPs occurs when accelerated inside a microfluidic channel by an externally applied magnetic field without flow, it is the indication of the presence (detection) of analyte (e.g., biomolecules) in the fluid under investigation. This percentage velocity decrease can be optimized if microparticles of smaller diameter (nm range) are utilized. Finally, one important factor of on chip particle manipulation devices that is often overlooked is the colloidal and surface forces acting among particles, defining whether a solution is stable or not, and between particles and surfaces. These forces are adequately defined by the DLVO interaction theory which suggests that the stability of a colloidal system is determined by the sum of the van der Waals attractive and electrical double layer repulsive forces that exist between particles as they

a)

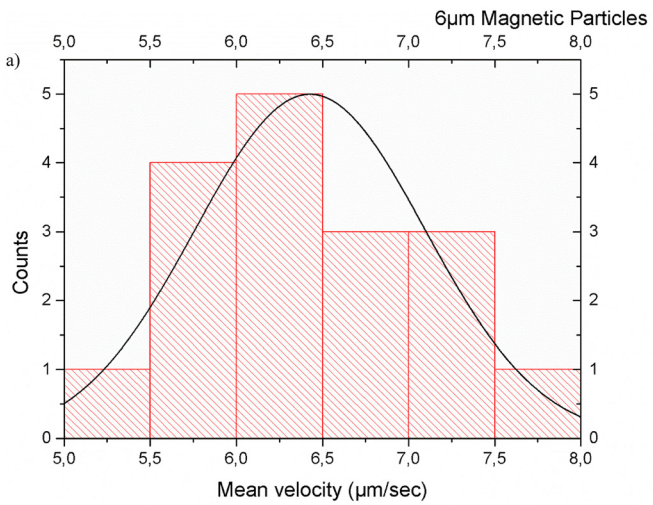

b)

	Statistical Mean	Standard Deviation	Minimum	Median	Maximum
Mean velocity	6,42795	0,6675	5,40541	6,25	7,69231

FIG. 10. (a) Graph showing the mean velocity of magnetic particles, SMPs, with a diameter of 6 μm versus the counts. (b) The values for statistical mean, standard deviation, minimum, median, and maximum are given in the table.

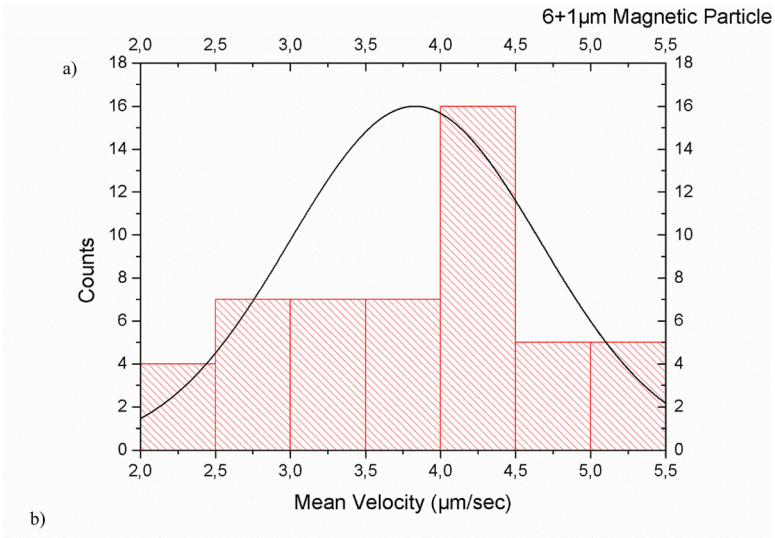

	Statistical Mean	Standard Deviation	Minimum	Median	Maximum
Mean velocity	3,8294	0,83493	2,22222	4	5,12821

FIG. 11. (a) Graph showing the mean velocity of magnetic particles, LSMPs, with a diameter of $6+1\,\mu$m versus the counts. (b) The values for statistical mean, standard deviation, minimum, median, and maximum are given in the table.

approach each other. In our experiments, enhancement of the electrostatic interaction was achieved by decreasing the electrolyte and the hydrogen ion concentration, meaning adjusting the solution at a pH 9 or higher. Although a steric stabilization approach is often preferable, for the described application a more basic solution is not inhibiter. The pH of the solution was adjusted by adding Hellmanex® at a dilution ratio 1:50 in DI water.

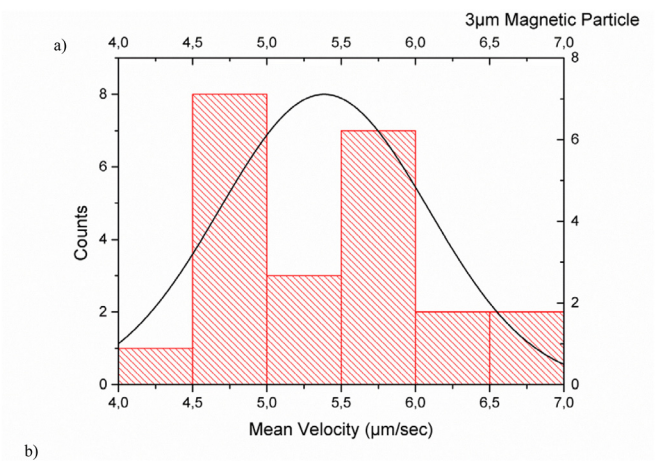

	Statistical Mean	Standard Deviation	Minimum	Median	Maximum
Mean velocity	5.3848	0.70015	4.4444	5.3333	6.6666

FIG. 12. (a) Graph showing the mean velocity of magnetic particles, SMPs, with a diameter of $3\,\mu$m versus the counts. (b) The values for statistical mean, standard deviation, minimum, median, and maximum are given in the table.

a)

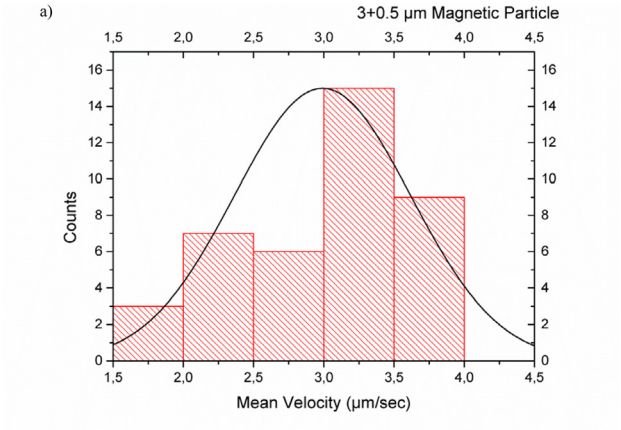

b)

	Statistical Mean	Standard Deviation	Minimum	Median	Maximum
Mean velocity	2.9907	0.6269	1.5778	3.1688	3.9026

FIG. 13. (a) Graph showing the mean velocity of magnetic particles, LSMPs, with a diameter of $3 + 0.5\,\mu$m versus the counts. (b) The values for statistical mean, standard deviation, minimum, median, and maximum are given in the table.

V. CONCLUSIONS

The presented experiments proved that the proposed system can be successfully used for the detection of organic compounds conjugated with superparamagnetic particles. The possibility of using magnetic sensors for the detection of the movement of the magnetic microparticles instead of optical detection is currently being investigated. Additionally, the possibility to use the principal of operation of the presented device as a filtering mechanism that would separate SMPs and LSMPs when inside the same microfluidic channel will be considered for future investigations. Setting up an actuation time adequate for the size of the SMPs, the LSMPs will fall back, thus separating them.

ACKNOWLEDGMENTS

The authors would like to acknowledge the financial support of the Austrian Science Fund (FWF) with Project No. P 24372-N19. The authors are grateful to Mr. Dietmar Puchberger-Enengl for the technical support.

[1]A. Arora, G. Simone, G. Salieb-Beugelaar, J. Kim, and A. Manz, Anal. Chem. **82**, 4830 (2010).
[2]M. Kovarik, P. Gach, D. Ornoff, Y. Wang, J. Balowski, L. Farrag, and N. Allbritton, Anal. Chem. **84**, 516 (2011).
[3]G. Antipas, E. Statharas, P. Tserotas, N. Papadopoulos, and E. Hristoforou, ChemPhysChem **14**, 1934 (2013).
[4]D. Graham, H. Ferreira, and P. Freitas, Trends Biotechnol. **22**, 455 (2004).
[5]M. Gijs, Microfluid. Nanofluid. **1**, 22 (2004).
[6]E. Hristoforou, J. Opt. Adv. Mater. **4**, 347 (2002).
[7]E. Hristoforou and A. Ktena, J. Magn. Magn. Mater. **316**, 372 (2007).
[8]B. Dufay, S. Saez, C. Cordier, C. Dolabdjian, C. Dubuc, E. Hristoforou, and S. Ubizskii, IEEE Sens. J. **11**, 3211 (2011).
[9]A. Sofla, B. Cirkovic, A. Hsieh, J. W. Miklas, N. Filipovic, and M. a Radisic, Biomicrofluidics **7**, 014110 (2013).
[10]H.-S. Moon, K. Kwon, K.-A. Hyun, T. S. Sim, J. C. Park, J.-G. Lee, and H.-I. Jung, Biomicrofluidics **7**, 014105 (2013).
[11]I. Cima, C. W. Yee, F. S. Iliescu, W. M. Phyo, K. H. Lim, C. Iliescu, and M. H. Tan, Biomicrofluidics **7**, 011810 (2013).
[12]L. Liang, J. Zhu, and X. Xuan, Biomicrofluidics **5**, 034110 (2011).
[13]D. Puchberger-Enengl, S. Podszun, H. Heinz, C. Hermann, P. Vulto *et al.*, Biomicrofluidics **5**, 044111 (2011).
[14]A. Dangl, G. Kokkinis, F. Keplinger, and I. Giouroudi, in *Conference Proceedings Nanotech Conference & Expo 2013, Washington, USA, 12–16 May* (2013), Vol. 3.
[15]I. Giouroudi, G. Kokkinis, C. Gooneratne, and J. Kosel, in *29th Southern Biomedical Engineering Conference Proceedings, Florida, USA, 3–5 May* (2013).
[16]C. Liu, L. Lagae, and G. Borghs, Appl. Phys. Lett. **90**, 184109 (2007).
[17]R. Wirix-Speetjens and J. De Boeck, IEEE Trans. Magn. **40**(4), 1944 (2004).
[18]N. Danckwardt, M. Franzreb, A. Guber, and V. Saile, J. Magn. Magn. Mater. **323**, 2776 (2011).

[19]I. Giouroudi, S. Van den Driesche, J. Kosel, R. Grössinger, and M. Vellekoop, J. Appl. Phys. **109**, 07B304 (2011).
[20]N. Pamme, Lab Chip **6**, 24 (2006).
[21]P. Hiemenz, *Principles of Colloidal and Surface Chemistry*, 3rd ed. (Marcel Dekker, Inc., New York, 1997).
[22]N. Nguyen and S. Wereley, *Fundamentals and Applications of Microfluidics* (Artech House, Inc., Norwood, 2002).
[23]C. Liu, L. Lagae, R. Wirix-Speetjens, and G. Borghs, J. Appl. Phys. **101**(2), 024913 (2007).
[24]C. Derec, C. Wilhelm, J. Servais, and J. Bacri, Microfluid. Nanofluid. **8**, 123 (2010).
[25]G. Hidy, *Aerosols: An Industrial and Environmental Science* (Academic Press, Inc., London, 1984).
[26]A. Lerman, *Geochemical Processes: Water and Sediment Environments* (Wiley, Oxford, 1979).
[27]J. Israelachvili, *Intermolecular and Surface Forces*, 3rd ed. (Elsevier, Burlington, USA, 2010).
[28]I. Giouroudi and F. Keplinger, Int. J. Mol. Sci. **14**, 18535–18556 (2013).
[29]C. Gooneratne, C. Liang, I. Giouroudi, and J. Kosel, "An integrated micro-chip for rapid detection of magnetic particles," J. Appl. Phys. **111**, 07B327 (2012).
[30]C. Gooneratne, I. Giouroudi, and J. Kosel, "A planar conducting micro-loop structure for transportation of magnetic beads: An approach towards rapid sensing and quantification of biological entities," Sens. Lett. **10**, 770–774 (2012).
[31]A. Rida, V. Fernandez, and M. Gijs, Appl. Phys. Lett. **83**, 2396 (2003).